

# Simultaneous Reduction of Pressure Rise Rate and Emissions in a Compression Ignition Engine by Use of Dual-Component Fuel Spray

Yoshimitsu Kobashi, Hiroki Maekawa and Satoshi Kato  
Kanazawa Institute of Technology

Jiro Senda  
Doshisha University

## ABSTRACT

Ignition, combustion and emissions characteristics of dual-component fuel spray were examined for ranges of injection timing and intake-air oxygen concentration. Fuels used were binary mixtures of gasoline-like component i-octane (cetane number 12, boiling point 372 K) and diesel fuel-like component n-tridecane (cetane number 88, boiling point 510 K). Mass fraction of i-octane was also changed as the experimental variable. The experimental study was carried out in a single cylinder compression ignition engine equipped with a common-rail injection system and an exhaust gas recirculation system. The results demonstrated that the increase of the i-octane mass fraction with optimizations of injection timing and intake oxygen concentration reduced pressure rise rate and soot and NO<sub>x</sub> emissions without deterioration of indicated thermal efficiency. Numerical investigation into the pressure rise rate reduction mechanism was also performed by use of a multi-component fuel model developed by the authors. The calculated result showed that the pressure rise rate was reduced due to the difference in the vapor concentrations between two components which have difference reactivity.

**CITATION:** Kobashi, Y., Maekawa , H., Kato, S. and Senda, J., "Simultaneous Reduction of Pressure Rise Rate and Emissions in a Compression Ignition Engine by Use of Dual-Component Fuel Spray," *SAE Int. J. Fuels Lubr.* 5(3):2012, doi: 10.4271/2012-32-0031.

## INTRODUCTION

Premixed charge compression ignition (PCCI) using early or late direct injection, high pressure injection and exhaust gas recirculation (EGR) offers promise for reducing particulate matter (PM) and NO<sub>x</sub> emissions while keeping diesel-like thermal efficiency [1,2,3]. However, several technical issues still must be resolved. Among these, controlling the combustion duration and hence the pressure rise rate is a major issue to extend the applicable operation range. It is generally agreed that the important parameters impacting the pressure rise rate are the combustion phasing and the charge stratification [4,5,6], although the combustion phasing retard is restricted by misfire or by deterioration of the thermal efficiency while the charge stratification often increases CO and NO<sub>x</sub> emissions [7]. Currently, as a realistic means, Shimazaki et al. [8] has proposed a dual mode combustion concept, in which engine is run with premixed charge operation from low till medium loads while diesel

mixing-controlled combustion is adapted for high load operation at which emissions are reduced by aftertreatment device.

To expand the load range of premixed charge operation and to achieve low emissions combustion at a high load, the authors have developed a combustion control method by use of physical and chemical properties of dual-component fuels [9, 10]. As schematically shown in Fig.1, a dual-component fuel consisting of different reactivity and volatility components provides a mixture in which two components are stratified due to the difference in the evaporation rate [11,12,13]. This so-called batch-distillation phenomenon can yield spatial-temporal difference in the ignition and combustion progress, associated with slowing of global combustion rate, and hence the premixed charge operation can be applied to higher load. Nevertheless, by increasing fuel loading, the range of the premixed charge operation could be limited by the increment of the combustion rate, so that mixing-controlled combustion would be employed

because of its ability to control the combustion rate. Although a major drawback of conventional mixing-controlled combustion is a trade-off relation between PM and NO<sub>x</sub>, mixing less reactive component increases lift-off length which is generally defined as a distance from nozzle tip to active combustion zone [14]. An increased lift-off length reduces the equivalence ratio in the diffusion flame, because the amount of entrained air increases with distance to nozzle, and hence reduces PM emissions [15].

Thus, in the present study, engine tests were carried out at a low load, focusing on the effect of mixing gasoline-like component into diesel-like component on pressure rise rate and emissions during premixed charge operation. In addition, to develop an understanding of the pressure rise rate reduction mechanism, a numerical investigation was also performed by use of a multi-component fuel model.

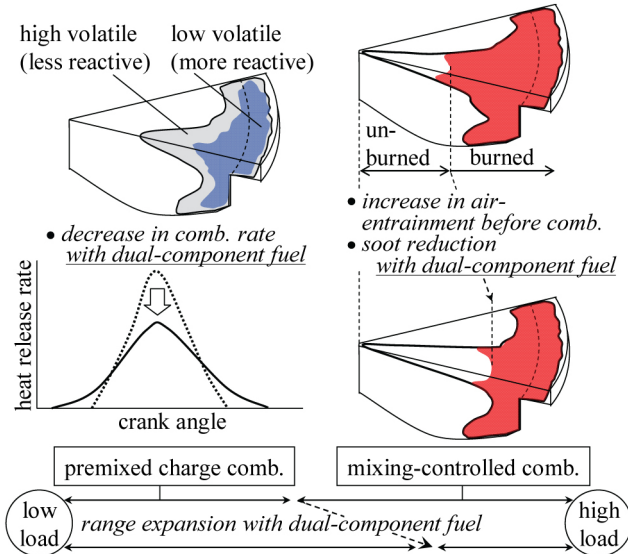


**Figure 1. Schematic illustration of controlled combustion rate and low emissions combustion strategy using dual-component fuel.**

## EXPERIMENTS

### Experimental Setup and Conditions

Experiments were carried out in a single cylinder, direct injection, water-cooled 4-stroke compression engine. The appearance of a piston is illustrated in Fig. 2. Specifications of the test engine and operating conditions are listed in Table 1. The test engine has dishshaped combustion chamber with the cavity diameter of 60 mm. The bore and the stroke are 83 mm and 85 mm, respectively. Temperatures of intake air, coolant water and lubricant oil were kept constant during the operation.

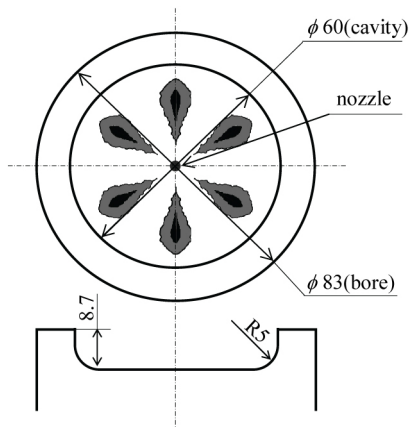


**Figure 2. Appearance of piston and its cavity geometry.**

**Table 1. Engine specification and experimental condition.**

Bore × Stroke	[mm]	83 × 85
Compression ratio	[ - ]	16.6
Engine speed	[rpm]	800
Intake air temperature	[K]	313 ± 1
Lubricant oil temperature	[K]	353 ± 1
Water temperature	[K]	353 ± 1
Injection pressure	[MPa]	70
Injection quantity, $Q_{inj}$ [mg/cycle]		8.6
Injection pulse timing, $\theta_{inj}$ [deg.CA ATDC]		from -25 to -5 as a step of 5 deg.CA
Intake oxygen concentration, $X_{O2}$ [vol.%]		21 and from 17 to 14 as a step of 1 vol.-%
Operating limitation		$dp/d\theta_{max} < 1.2 \text{ MPa/deg.CA}$ COV of IMEP < 6 %

A flush-mounted piezoelectric pressure transducer (KISTLER: 6125C01) was installed to measure in-cylinder pressure. The pressure data as well as injection pulse signal were recorded for 120 cycles, every 0.5 crank angle degree (deg.CA), based on the electric pulse from a rotary encoder. Exhaust gas concentrations of total-hydrocarbons (THC), CO, CO<sub>2</sub> and NO<sub>x</sub> were measured by an exhaust analyzer (HORIBA: MEXA-9100D). To measure the mass of particulate matter (PM) according to filter weighting method, the exhaust gas was diluted through a full-dilution tunnel before PM was collected on a Teflon filter. Soxhlet extractor was used to isolate soluble organic fraction (SOF) from PM, and then insoluble fraction (ISF) which is predominantly composed of soot was evaluated.

Intake oxygen concentration ( $X_{O2}$ ) was changed as an experimental variable by recirculating a portion of engine exhaust gases back to the cylinder and the  $X_{O2}$  was measured by the above exhaust gas analyzer. Before leading the gases to intake manifold, PM emissions were removed through a

diesel particulate filter and gases temperature was lowered to around intake air temperature by an EGR cooler.

A commercially available common-rail fuel injection system was used for direct injection. Fuel temperature was kept around 293 K with heat exchanger to suppress bubble release in the fuel line. The injector nozzle has 6 orifices with an umbrella angle of 145 degree (17.5 degree down-angle from the bottom surface of the cylinder head and their nominal diameter is 0.16 mm. Five different injection pulse timings ( $\theta_{inj}$ ) from -25 deg.CA ATDC to -5 deg.CA ATDC were selected.

An injected fuel quantity was 8.6 mg/cycle. This corresponds to global equivalence ratio of 0.26 without taking into account exhaust gas recirculation. Though the resulting indicated mean effective pressure (IMEP) varied according to the experimental condition, the maximum IMEP for all the experiments was about 0.33 MPa.

## Fuels Tested

N-tridecane (n-C<sub>13</sub>H<sub>28</sub>) which is more reactive (cetane number 88) and high boiling point (boiling point 510 K) was used as a diesel-like component. By mixing i-octane (i-C<sub>8</sub>H<sub>18</sub>) which is less reactive (cetane number 12) and low boiling point (boiling point 372 K) into n-C<sub>13</sub>H<sub>28</sub>, the effect of a gasoline-like component was examined. The present study set the mass fraction of i-C<sub>8</sub>H<sub>18</sub> ( $M_{iC8}$ ) as 0 (pure n-C<sub>13</sub>H<sub>28</sub>), 50, 70 and 80 wt.%. As denoted above, the global equivalence ration was 0.26. As for  $M_{iC8}$  of 50, 70 and 80 wt.%, the equivalence ratios of n-C<sub>13</sub>H<sub>28</sub> were 0.13, 0.08 and 0.05, and those of i-C<sub>8</sub>H<sub>18</sub> were 0.13, 0.18 and 0.21, respectively.

## MULTI-COMPONENT FUEL MODEL

The multi-component fuel model has been developed based on KIVA3V [16]. Since more detailed description is found in the literatures [13, 17], essential points are described here.

## Droplet Breakup and Evaporation

In order to accurately predict liquid phase penetration, the Kelvin-Helmholtz and Rayleigh-Taylor (KH-RT) model [18] was incorporated as a droplet breakup model. Same KH-RT model constants were adopted despite the fuels.

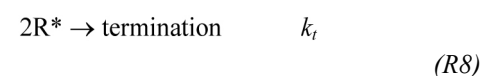
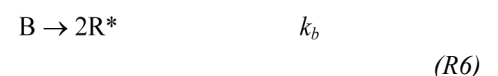
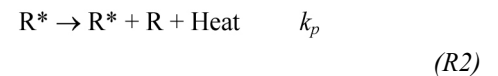
To evaluate the effects of interaction between molecules, high-pressure and non-ideal gas on phase properties and droplet evaporation process, a source code of SURERTRAPP [19] developed in National Institute of Standards and Technology was incorporated into KIVA3V. The SUPERTRAPP code calculates vapor-liquid equilibrium and gives phase compositions with Peng-Robinson equation of state. The solubility of ambient gas in the droplet was taken into account, while omitting internal circulation of the liquid and temperature gradient within the droplet.

## Estimation of Physical Properties

Due to the difference in the evaporation rate among components, the mixture fraction within the droplet is changed as time goes by. Thus, all the fuel properties of droplet parcels were updated in every numerical timestep with taking into account both temperature and pressure effects as well as mixing fraction. The SUPERTRAPP code calculates thermodynamic and transport properties based on extended corresponding states. The more details on the prediction method are found in the literatures [17, 20].

## Ignition and Combustion Models

The oxidation reaction lower than 1000 K was solved by the multistep kinetics Shell ignition model [21]. It includes eight reaction steps between five generalized species, specified as:



where RH indicates the fuel, R\* is the generalized radical, Q is an unstable intermediate agent, B is the branching agent, and P denotes oxidized products such as CO, CO<sub>2</sub> and H<sub>2</sub>O. The rate terms  $f_i$  are expresses as follows:

$$f_i = A_{f_i} \cdot \exp\left(\frac{-E_{f_i}}{R \cdot (T - T_x)}\right) \cdot [\text{O}_2]^{x_i} \cdot [\text{RH}]^{y_i} \quad (1)$$

where R is universal gas constant, T is cell temperature and  $T_x$  is a correction for temperature described below. The kinetic parameters,  $k_q$ ,  $k_b$  and  $k_t$ , are expressed in the Arrhenius form as:

$$k_i = A_i \cdot \exp\left(\frac{-E_{f_i}}{R \cdot (T - T_x)}\right) \quad (2)$$

$k_p$  is given by the following expression with three rate coefficients:

$$k_p = \left[ \frac{1}{k_{p_1} \cdot [\text{O}_2]} + \frac{1}{k_{p_2}} + \frac{1}{k_{p_3} \cdot [\text{RH}]} \right]^{-1} \quad (3)$$

The species concentrations are solved by numerically integrating the differential equations. The heat release can be expressed by the reaction (R2). For the implementation of multi-dimensional simulation, the Shell model was modified to maintain the mass conservation according to the procedure of Schäpertöns and Lee [22].

In the ignition and combustion simulation of multi-component fuel spray, the mixture compositions are different among computational cells since each component evaporates at different rate. Thus, the reaction should be solved in all the cells. The previous study [17] solved the above rate equations independently for each fuel component, ignoring chemical interaction between the components. Shell model constants of PRF90 proposed by Theobald and Cheng [23] were employed. The difference in the chemical reaction rates between the fuels was taken into account by the activation energy  $E_{f4}$  in Eq.(1) and by the rate term  $f_4$  in (R4) as follows:

$$E^* f_i = E_{f_i} \frac{a}{CN + b} \quad (4)$$

where CN is cetane number and  $a$  and  $b$  are constants determined to fit to the ignition delay of the detailed chemical kinetic calculation.

A correction for temperature  $T_x$  was also included in Eq.(1) and Eq.(2) according to the procedure established by Nakama et al. [24], because the model constants were determined for mean gas temperature in a combustion chamber while there is actually temperature gradient.  $T_x=80$  K [25] was set as the difference between the average temperature and the core temperature.

i-C<sub>8</sub>H<sub>18</sub> utilized in the present study is so-called PRF100 so that Shell model constants of PRF100 [23] were selected. Unfortunately, in the case of n-C<sub>13</sub>H<sub>28</sub>, PRF100 model constants with the modification of  $E_{f4}$  through Eq.(4) could not adequately reproduce the ignition delay of detailed chemistry. In contrast, by adjusting  $E_{f1}$  in Eq.(1) and the rate term  $f_1$  in (R3) through Eq.(4), the ignition delay predicted by PRF100 model constants could be in good agreement with that of detailed chemistry. Thus, the present study adopts the latter method to take into account the difference in the chemical reaction rates between the fuels.

Figure 3 compares ignition delays in Arrhenius form between Shell model and CHEMKIN-II [26] predictions at constant volume. The calculation was implemented under pressure of 3.6 MPa. To determine the ignition delay of n-C<sub>13</sub>H<sub>28</sub> and i-C<sub>8</sub>H<sub>18</sub>, detailed mechanisms of Lawrence

Livermore National Laboratory [27, 28] were utilized in the CHEMKIN calculation, while Shell model prediction was run as described above. The Shell predictions qualitatively reflect the change in ignition delay with temperature, equivalence ratio and fuel, although the discrepancy becomes clear with the increase of the equivalence ratio.

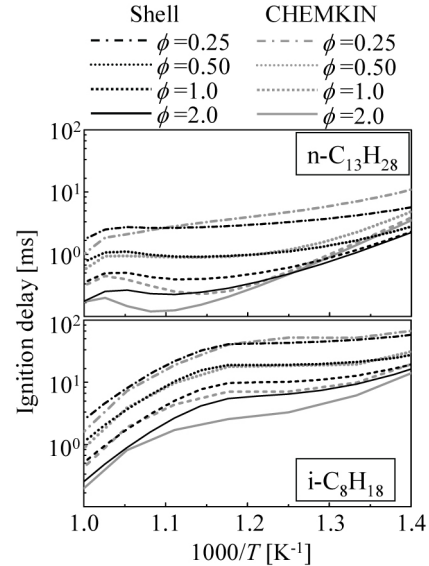


Figure 3. Comparison of ignition delay between calculations using Shell model and CHEMKIN

A simple single step oxidation model pre-installed into KIVA3V was used to predict oxidation reactions higher than 1000 K. Based on the local compositions at each cell, the dual-component species were assumed to be a mole-averaged single fuel. The eddy-dispersion model developed by Magnussen et al. [29] was used to consider the turbulent mixing-controlled combustion.

## RESULT AND DISCUSSION

### Operating Range and Combustion Characteristics

Figure 4 shows the contour map of maximum pressure rise rate ( $dp/d\theta_{max}$ ) and operating range for all the experimental conditions. In this figure, the horizontal axis is injection pulse timing ( $\theta_{inj}$ ) and the vertical axis is intake oxygen concentration ( $X_{O2}$ ). The black dots shown in the figure are the experimental points. For all the fuels tested, the  $dp/d\theta_{max}$  increased with advancing the  $\theta_{inj}$  and the increase of the  $X_{O2}$ . The severe  $dp/d\theta_{max}$  which was higher than 1.2 MPa/deg.CA expanded toward later  $\theta_{inj}$  and lower  $X_{O2}$  conditions with the increase of i-C<sub>8</sub>H<sub>18</sub> mass fraction ( $M_{iC8}$ ) from 0 wt.% to 50 wt.%, while the severe  $dp/d\theta_{max}$  conditions decreased with the increase of  $M_{iC8}$  from 50 wt.% to 80 wt.%. Meanwhile, the higher  $M_{iC8}$  was likely to cause

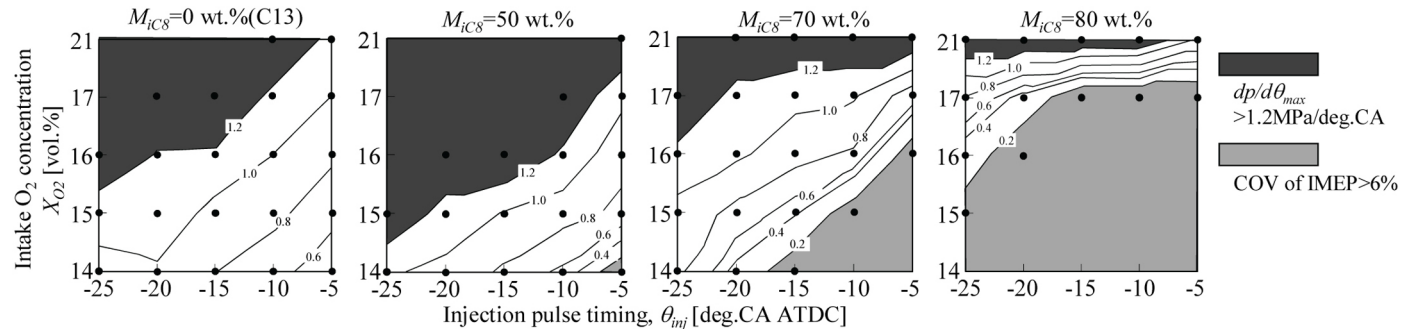
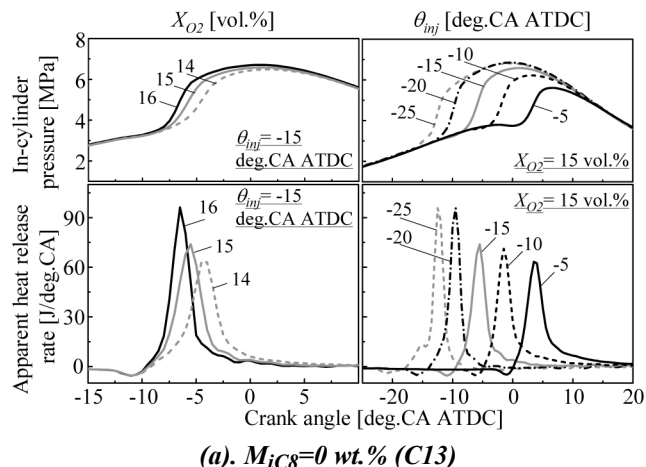


**Figure 4. Contour map of maximum pressure rise rate,  $dp/d\theta_{max}$ , and operating range for all experimental conditions.**

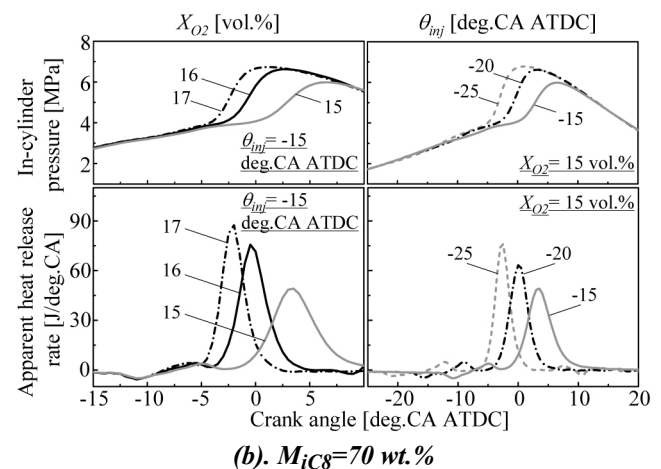
unacceptable cycle fluctuation under the later  $\theta_{inj}$  and lower  $X_{O2}$  conditions.

As for (a)  $M_{iC8}=0$  wt.% (pure n-C<sub>13</sub>H<sub>28</sub>) and (b)  $M_{iC8}=70$  wt.%, the histories of the in-cylinder pressure and the apparent heat release rates (AHRR) are shown in Fig.5. The left side figures show the variation of the AHRR with  $X_{O2}$  under the fixed  $\theta_{inj}$ , while the right side figures show that with  $\theta_{inj}$  under the fixed  $X_{O2}$ . Despite the fuels, the decrease of the  $X_{O2}$  retarded the combustion phasing and decreased the peak of the AHRR. Also, the early  $\theta_{inj}$  advanced the combustion phasing and increased the peak of the AHRR due to the enhanced mixing.

By comparing the AHRRs between the fuels under the same operating conditions, the combustion phasing of  $M_{iC8}=70$  wt.% was later than that of  $M_{iC8}=0$  wt.%. In addition, the AHRR peak of the former is lower than that of the latter. Such a slower and retard combustion of dual-component fuels was likely to cause unstable combustion. However, mixing i-C<sub>8</sub>H<sub>18</sub> could contribute to the reduction of the combustion rate and hence of the  $dp/d\theta_{max}$  and to the range expansion of premixed charge operation. Thus, the  $dp/d\theta_{max}$  reduction mechanism will be discussed through a numerical simulation in the next sub-section.



**(a).  $M_{iC8}=0$  wt.% (C13)**



**(b).  $M_{iC8}=70$  wt.%**

**Figure 5. Variations of in-cylinder pressure and apparent heat release rate with injection pulse timing,  $\theta_{inj}$ , and intake oxygen concentration,  $X_{O2}$ , for pure n-C<sub>13</sub>H<sub>28</sub> ( $M_{iC8}=0$  wt.%) and dual-component fuel ( $M_{iC8}=70$  wt.%).**

## Mechanism of Pressure Rise Rate Reduction due to Dual-Component Fuel

The model validation has already been conducted in terms of spray tip penetration, liquid length, ignition delay and heat release rate of dual-component fuel sprays formed in a constant volume combustion chamber [17]. For further evaluation, the accuracy for the ignition timing and combustion phasing in a single cylinder engine as well as for new Shell model constants was investigated by comparing heat release rate between experiments and predictions. Figure 6 illustrates the computational domain representing the single cylinder engine used in the experiments.

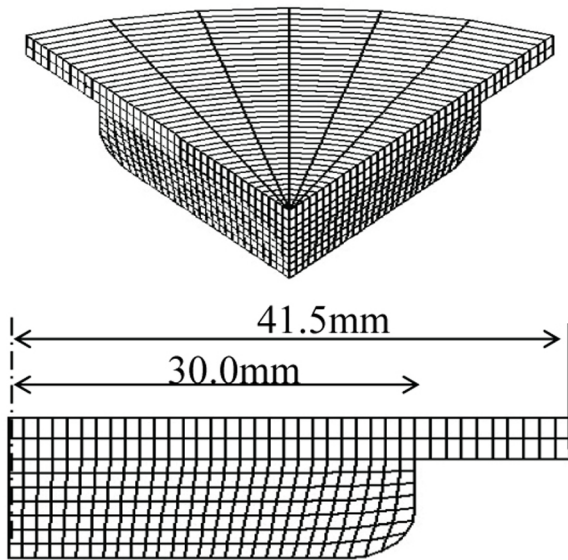


**Figure 6. Computational domain**

Figure 7 are the predicted histories of heat release rate under  $\theta_{inj} = -20$  deg.CA ATDC and  $X_{O2} = 15$  vol.%, compared with the experimental ones. It should be noted that the experimental result shows the apparent heat release rate calculated from measured in-cylinder pressure which included heat loss, while the net heat release rate which equals to the heat generated by chemical exothermic reactions is shown as the predicted result. Due to the difference, the predicted net heat release rate is higher than the experimentally-obtained heat release rate. Apart from this discrepancy, however, the predicted ignition timing and combustion phasing were in good agreement with the experiments. Therefore, the effect of two components distribution on ignition and combustion processes was studied by use of the present prediction.

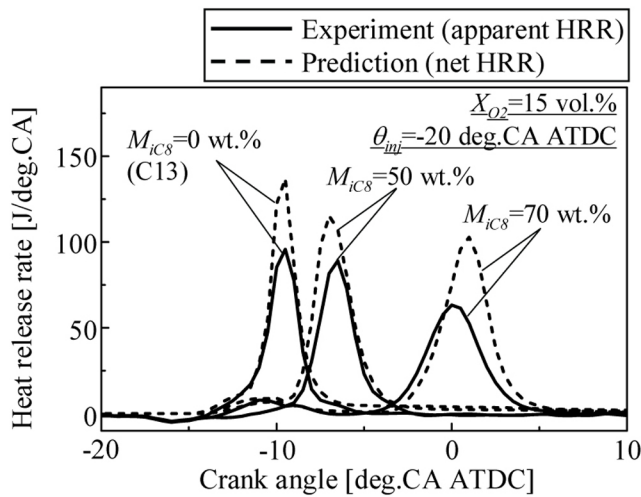


**Figure 7. Comparison of heat release rate between experiment and prediction for three fuels**

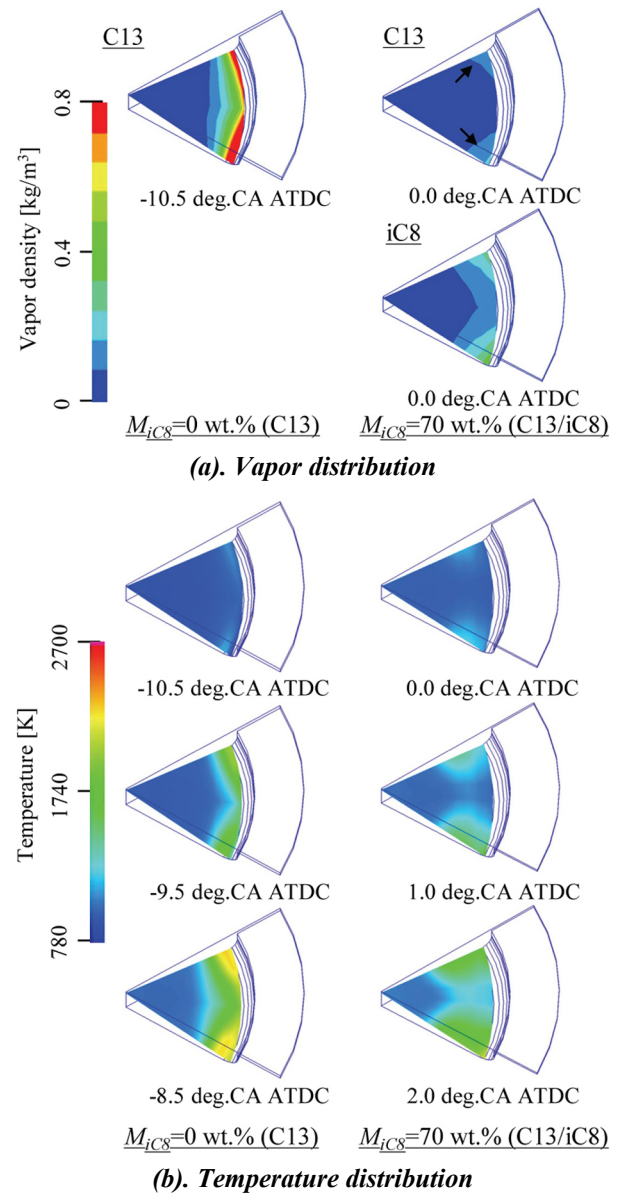


**Figure 8. Predicted distributions of vapors and temperature for pure n-C<sub>13</sub>H<sub>28</sub> ( $M_{iC8}=0$  wt.%) and dual-component fuel ( $M_{iC8}=70$  wt.%).**

Distributions of (a) vapor concentration and (b) temperature in the combustion chamber are displayed in Fig. 8. The calculation condition is identical with Fig. 7. For obtaining vapor concentration images of (a), the Shell and single-step combustion models were switched off. The vapor of pure n-C<sub>13</sub>H<sub>28</sub> ( $M_{iC8}=0$  wt.%) was seen along the piston cavity wall with relatively high concentration. Consequently, once the ignition occurred along the wall, the gas temperature promptly increased, elevating the heat release rate. In the case of  $M_{iC8}=70$  wt.%, the vapor of n-C<sub>13</sub>H<sub>28</sub> was seen in local position indicated by the arrows while i-C<sub>8</sub>H<sub>18</sub> formed the vapor with the wider and leaner distribution than  $M_{iC8}=0$  wt. %. At 0.0 deg.CA ATDC, the ignition occurred at the side

edges of the image where n-C<sub>13</sub>H<sub>28</sub> was distributed. And then, combustion zone was gradually spread toward the entire area of the chamber, involving the combustion of i-C<sub>8</sub>H<sub>18</sub> vapor. It seems that such a spatial-temporal difference in the combustion phasing between the n-C<sub>13</sub>H<sub>28</sub> and i-C<sub>8</sub>H<sub>18</sub> reduced the heat release rate and stretched the combustion duration.

In fact, however, there were the differences in ignition delay and volatility between  $M_{iC8}=0$  wt.% and 70 wt.%. Since these factors can affect mixture concentration and hence combustion rate, further investigation into the effect of them on the  $dp/d\theta_{max}$  was conducted. In Fig.9, the relation between the measured  $dp/d\theta_{max}$  and mixing duration is shown. The peak of apparent heat release rate was also employed as an indicator of the combustion rate. The mixing duration was defined as the interval between the injection pulse timing,  $\theta_{inj}$ , and the crank angle at which heat release rate reached the peak.

Despite the fuels, stretching the mixing duration was associated with the increase in the peak of heat release rate and in the  $dp/d\theta_{max}$ . This is due to the fact that the long mixing duration increased the amount of combustible mixture and enhanced homogenization of mixture by the onset of ignition. Mixing i-C<sub>8</sub>H<sub>18</sub> increased the ignition delay. Nevertheless, it reduced the peak of heat release rate and the  $dp/d\theta_{max}$ . Consequently, the authors conclude that the mechanism of  $dp/d\theta_{max}$  reduction is due to the mixture distribution, ignition and combustion characteristics.

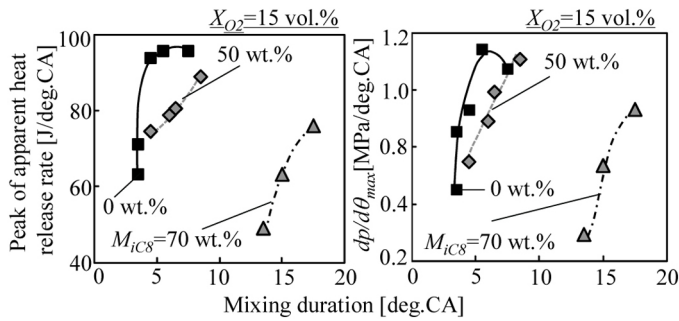


**Figure 9. Relation between mixing duration and peak of apparent heat release rate and maximum pressure rise rate,  $dp/d\theta_{max}$  measured**

## Emissions Characteristics and Indicated Thermal Efficiency

Figure 10 summarizes measured exhaust emissions and combustion efficiency,  $\eta_c$ . The data shown was obtained for all the fuels under  $\theta_{inj}=-5$ , -15 and -25 deg.CA ATDC. The decrease in the  $X_{O2}$  reduced NO<sub>x</sub> and  $\eta_c$  due to the decrease in the combustion temperature and to the long ignition delay. As for pure n-C<sub>13</sub>H<sub>28</sub> ( $M_{iC8}=0$  wt.%), the deterioration of the  $\eta_c$  was pronounced for the late injection ( $\theta_{inj}=-5$  deg.CA

ATDC). This can be attributed to the increase of CO, derived from rich mixture. ISF was detected only under  $\theta_{inj}=-5$  deg.CA ATDC and the  $X_{O2}$  higher than 16 vol.%. In other words, the conditions with early injection and/or low intake oxygen concentration had less ISF emission.

Mixing i-octane reduced NO<sub>x</sub> and ISF emissions as well as  $\eta_c$ . This is due to the fuel volatility and the stretched ignition, which can enhance the lean mixture formation. The reactivity of i-C<sub>8</sub>H<sub>18</sub> was likely to be a factor increasing the THC emissions. However, the deterioration of the combustion efficiency was less notable for the early injection because the long ignition delay prevented CO formation.

The indicated thermal efficiency,  $\eta_i$ , for all the fuels is shown in Fig.11. The  $\eta_i$  of  $M_{iC8}=0$  wt.% was deteriorated with the advanced  $\theta_{inj}$ , because the early injection advanced the combustion phasing, increasing negative work as shown in Fig.5. The decrease of  $X_{O2}$  deteriorated the combustion efficiency, nonetheless, it slightly increased  $\eta_i$  except for the latest injection of  $\theta_{inj}=-5$  deg.CA ATDC. This result suggests that the change in the combustion phasing plays an important role in  $\eta_i$ . It is also clear, however, that the  $X_{O2}$  has a minor role compared to the  $\theta_{inj}$ . Similar trend was seen in  $M_{iC8}=50$  wt.%.

The highest  $\eta_i$  of  $M_{iC8}=70$  wt.% was achieved with the earliest injection of  $\theta_{inj}=-25$  deg.CA ATDC and the lowest intake oxygen of  $X_{O2}=14$  vol.%. As described above, the early injection can mitigate the deterioration of the combustion efficiency. In addition, due to the long ignition delay, the early injection could set the combustion phasing closer to top dead center.  $M_{iC8}=80$  wt.% has the further long ignition delay so that the higher intake oxygen of  $X_{O2}=16$  vol.% was required to advance the combustion phasing and to achieve the highest  $\eta_i$ .

## Discussion on Maximum Pressure Rise Rate and Emissions

As discussed above, more reactive n-C<sub>13</sub>H<sub>28</sub> achieves high thermal efficiency with late injection, while mixing less reactive i-C<sub>8</sub>H<sub>18</sub> retards the injection pulse timing best for the thermal efficiency. Although such a long ignition delay increases the maximum pressure rise rate (see Fig.9), vapor distribution and combustion characteristics of dual-component fuel suppress the combustion rate (see Fig.7 and Fig.8). Thus, here in this sub-section, maximum pressure rise rate and emissions are compared between the fuels with taking into consideration the difference in the proper operating condition.

It should be noted, however, that the experiments were carried out within limited conditions, i.e., injection pulse timing as a step of 5 deg.CA and intake oxygen concentration as a step of 1 vol.%, so that the further precise optimization can lead higher indicated thermal

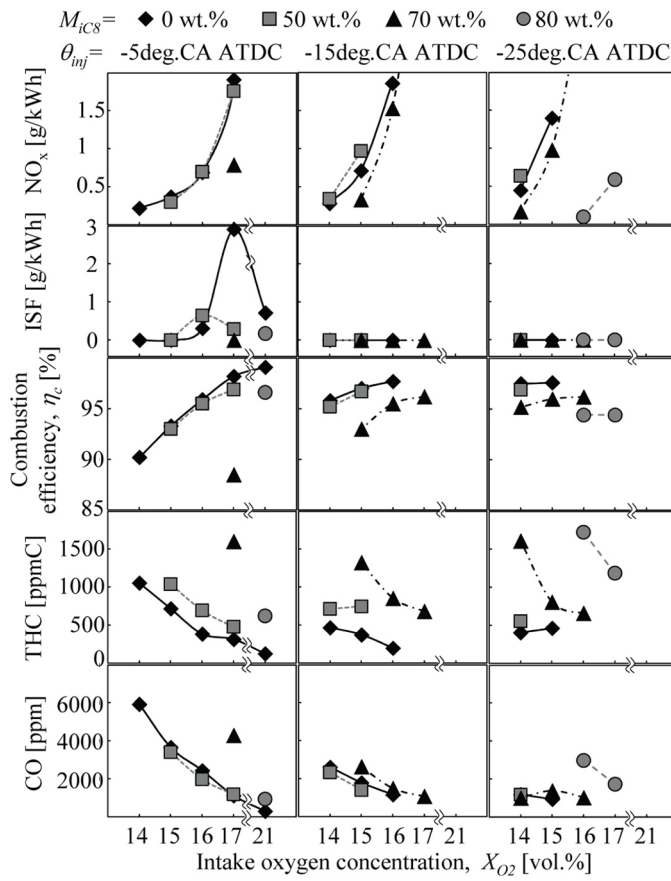


**Figure 10. Measured exhaust emissions and combustion efficiency**

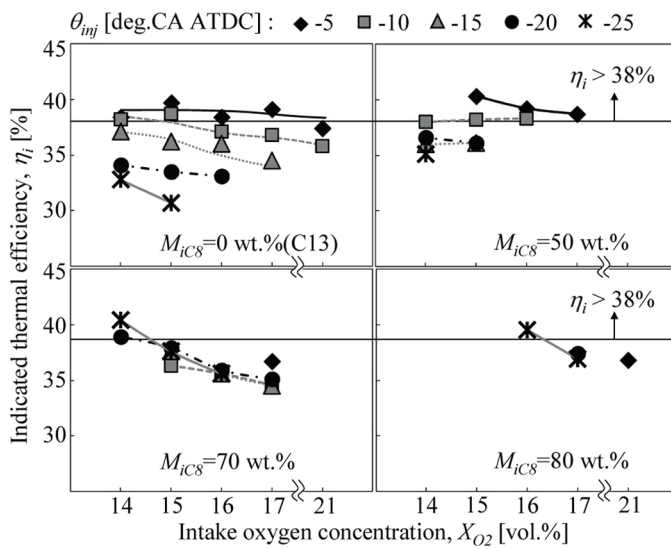


**Figure 11. Measured indicated thermal efficiency,  $\eta_i$ , for all experimental conditions**

efficiency. Thus, the data which achieves thermal efficiency above threshold level (38 %) was extracted and used for evaluation. Figure 12 shows the relation between  $NO_x$  and

ISF and  $dp/d\theta_{max}$  for all the fuels.  $M_{iC8}=0$  wt.% and 50 wt.% produced ISF in some of the conditions, while few ISF was found under the low  $dp/d\theta_{max}$  conditions.  $M_{iC8}=0$  wt.% and 50 wt.% showed a trend in which  $NO_x$  increased with the increase of the  $dp/d\theta_{max}$ . Increasing the mass fraction of i-C<sub>8</sub>H<sub>18</sub> reduced  $NO_x$ .  $M_{iC8}=0$  wt.% and 50 wt.% which achieve high thermal efficiency with late injection seemed to contain mixture ranging from rich to lean, as inferred from CO trend in Fig.10. In contrast,  $M_{iC8}=70$  wt.% and 80 wt.% which achieve high thermal efficiency with early injection seemed to contain lean mixture due to long mixing duration as well as the high volatility, and hence are likely to reduce  $NO_x$  and ISF. Consequently, although it was possible for a part of operating conditions of  $M_{iC8}=0$  wt.% to simultaneously reduce  $NO_x$  and ISF and  $dp/d\theta_{max}$ ,  $M_{iC8}=70$  wt.% and 80 wt.% were capable of reducing further. It should also be noted that the present experiments were carried out in a low load. The difference between the fuels may become obvious at higher operating load.

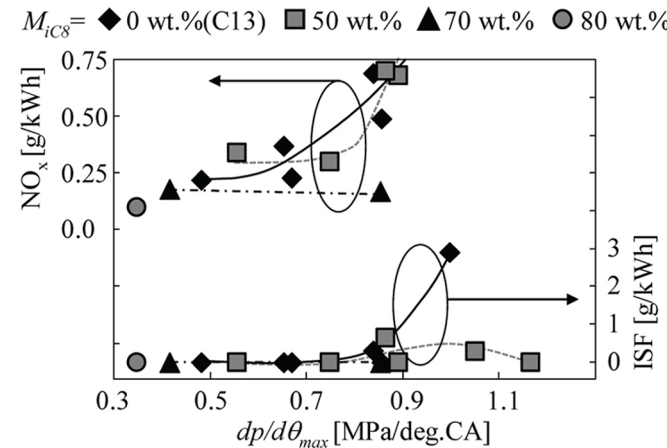


**Figure 12. Comparison of  $NO_x$  and ISF trends for maximum pressure rise rate,  $dp/d\theta_{max}$ , between all fuels tested (indicated thermal efficiency,  $\eta_i > 38\%$ )**

## CONCLUSIONS

The present paper carried out the single cylinder engine experiments using dual-component fuels consisting of n-C<sub>13</sub>H<sub>28</sub> and i-C<sub>8</sub>H<sub>18</sub>. By changing the fuel injection timing and intake oxygen concentration as well as using multi-component fuel model, the effects of mixture distribution on ignition and combustion characteristics were examined. The conclusions are as follows:

1. More reactive n-C<sub>13</sub>H<sub>28</sub> achieves high thermal efficiency with late injection timing close to top dead center, while dual-component fuel consisting of less reactive i-C<sub>8</sub>H<sub>18</sub> improves thermal efficiency by advancing injection timing near -25 deg.CA ATDC.

**2.** Maximum pressure rise rate of dual-component fuel is low even under early injection conditions despite the fact that early injection forms homogeneous mixture due to long mixing duration.

**3.** Above conclusion #2 is attributed to the fact that the two components locally have different vapor concentrations each other, because such a mixture causes the spatial-temporal difference in the combustion phasing and hence reduces global heat release rate.

**4.** Due to conclusion #1 as well as the high volatility, dual-component fuels are capable of reducing NO<sub>x</sub> and ISF (predominantly composed of soot) compared to single component of n-C<sub>13</sub>H<sub>28</sub>.

## REFERENCES

1. Aoyama, T., Hattori, Y., Mizuta, J., and Sato, Y., "An Experimental Study on Premixed-Charge Compression Ignition Gasoline Engine," SAE Technical Paper 960081, 1996, doi:[10.4271/960081](https://doi.org/10.4271/960081).
2. Kimura, S., Aoki, O., Kitahara, Y., and Aiyoshizawa, E., "Ultra-Clean Combustion Technology Combining a Low-Temperature and Premixed Combustion Concept for Meeting Future Emission Standards," SAE Technical Paper 2001-01-0200, 2001, doi:[10.4271/2001-01-0200](https://doi.org/10.4271/2001-01-0200).
3. Akihama, K., Takatori, Y., Inagaki, K., Sasaki, S. et al., "Mechanism of the Smokeless Rich Diesel Combustion by Reducing Temperature," SAE Technical Paper 2001-01-0655, 2001, doi:[10.4271/2001-01-0655](https://doi.org/10.4271/2001-01-0655).
4. Kumano, K. and Iida, N., "Analysis of the Effect of Charge Inhomogeneity on HCCI Combustion by Chemiluminescence Measurement," SAE Technical Paper 2004-01-1902, 2004, doi:[10.4271/2004-01-1902](https://doi.org/10.4271/2004-01-1902).
5. Sjöberg, M., Dec, J., and Cernansky, N., "Potential of Thermal Stratification and Combustion Retard for Reducing Pressure-Rise Rates in HCCI Engines, Based on Multi-Zone Modeling and Experiments," SAE Technical Paper 2005-01-0113, 2005, doi:[10.4271/2005-01-0113](https://doi.org/10.4271/2005-01-0113).
6. Sjöberg, M. and Dec, J., "Smoothing HCCI Heat-Release Rates Using Partial Fuel Stratification with Two-Stage Ignition Fuels," SAE Technical Paper 2006-01-0629, 2006, doi:[10.4271/2006-01-0629](https://doi.org/10.4271/2006-01-0629).
7. Aroonsrisopon, T., Werner, P., Waldman, J., Sohm, V. et al., "Expanding the HCCI Operation With the Charge Stratification," SAE Technical Paper 2004-01-1756, 2004, doi:[10.4271/2004-01-1756](https://doi.org/10.4271/2004-01-1756).
8. Shimazaki, N., Tsurushima, T., and Nishimura, T., "Dual Mode Combustion Concept With Premixed Diesel Combustion by Direct Injection Near Top Dead Center," SAE Technical Paper 2003-01-0742, 2003, doi:[10.4271/2003-01-0742](https://doi.org/10.4271/2003-01-0742).
9. Senda, J., Kawano, D., Hotta, I., Kawakami, K. et al., "Fuel Design Concept for Low Emission in Engine Systems," SAE Technical Paper 2000-01-1258, 2000, doi:[10.4271/2000-01-1258](https://doi.org/10.4271/2000-01-1258).
10. Senda, J., Wada, Y., Kawano, D. and Fujimoto, H., "Improvement of Combustion and Emissions in Diesel Engines by Means of Enhanced Mixture Formation Based on Flash Boiling of Mixed Fuel", Int. J. Engine Research, Vol.9, No.1, pp.15-27, (2008)
11. Senda, J. and Fujimoto, H., "Multicomponent Fuel Consideration for Spray Evaporation Field and Spray-Wall Interaction," SAE Technical Paper 2001-01-1071, 2001, doi:[10.4271/2001-01-1071](https://doi.org/10.4271/2001-01-1071).
12. Kawano, D., Senda, J., Kawakami, K., Shimada, A. et al., "Fuel Design Concept for Low Emission in Engine Systems 3rd Report: Analysis of Spray Characteristics for Mixed Fuels," SAE Technical Paper 2002-01-0220, 2002, doi:[10.4271/2002-01-0220](https://doi.org/10.4271/2002-01-0220).
13. Kawano, D., Senda, J., Wada, Y., Fujimoto, H. et al., "Numerical Simulation of Multicomponent Fuel Spray," SAE Technical Paper 2003-01-1838, 2003, doi:[10.4271/2003-01-1838](https://doi.org/10.4271/2003-01-1838).
14. Siebers, D. and Higgins, B., "Flame Lift-Off on Direct-Injection Diesel Sprays Under Quiescent Conditions," SAE Technical Paper 2001-01-0530, 2001, doi:[10.4271/2001-01-0530](https://doi.org/10.4271/2001-01-0530).
15. Okada, M., Shigetomi, D., Matsumoto, M., Kobashi, Y. and Senda, J., "Effects of Fuel Composition on Flame Lift-off Length and Pollutant Formation in Dual-component Fuel Spray", submitted to COMODIA 2012.
16. Amsden, A. A., "KIVA3V: A Block-Structured KIVA Program for Engines with Vertical or Canted Valves", Los Alamos National Laboratory Report LA-13313-MS, (1997)
17. Kobashi, Y., Fujimori, K., Maekawa, H., Kato, S. et al., "Modeling of Auto-Ignition and Combustion Processes for Dual-Component Fuel Spray," SAE Int. J. Engines 4(2):2193-2206, 2011, doi:[10.4271/2011-24-0001](https://doi.org/10.4271/2011-24-0001).
18. Beale, J. C. and Reitz, R. D., "Modeling Spray Atomization with the Kelvin-Helmholtz/ Rayleigh-Taylor Hybrid Model", Atomization and Sprays, Vol.9, pp.623-650, (1999)
19. Ely, J. F. and Huber, M. L., "NIST Thermophysical Properties of Hydrocarbon Mixtures Database User's Guide", (1992)
20. Huber, M. L. and Hanley, J. M., The Corresponding-States Principle: Dense Fluid, Chapter 12, *Transport Properties of Fluids-Their Correlation, Prediction and Estimation*, Cambridge University Press, pp.283-295, (1996)
21. Halstead, M. P., Kirsch, L. J. and Quinn, C. P., "The Autoignition of Hydrocarbon Fuels at High Temperatures and Pressures - Fitting of a Mathematical Model", Combustion and Flame, Vol.30, pp.45-60, (1977)
22. Schäpertöns, H. and Lee, W., "Multidimensional Modelling of Knocking Combustion in SI Engines," SAE Technical Paper 850502, 1985, doi:[10.4271/850502](https://doi.org/10.4271/850502).
23. Theobald, M. A. and Cheng, W. K., "A Numerical Study of Diesel Ignition", ASME 87-FE-2, pp.1-11, (1987)
24. Nakama, K., Murase, E., Tsukakoshi, T., Kusaka, J. and Daisho, Y., "Optimization of Shell Model Parameters Using Gasoline Surrogate Scheme", Transactions of JSAE, Vol.37, No.5, pp.57-62, (in Japanese) (2006)
25. Hu, H. and Keck, J., "Autoignition of Adiabatically Compressed Combustible Gas Mixtures," SAE Technical Paper 872110, 1987, doi:[10.4271/872110](https://doi.org/10.4271/872110).
26. Kee, R. J., Rupley, F. M. and Miller, J. A., "CHEMKIN-II: A Fortran Chemical Kinetics Package for the Analysis of a Gas-phase Chemical Kinetics", Sandia Laboratories Report, SAND 89-8009B, (1989)
27. Curran, H. J., Gaffuri, P., Pitz, W. J. and Westbrook, C. K., "Comprehensive Modeling Study of Iso-octane Oxidation", Combustion and Flame, Vol.129-3, pp.253-280, (2002)
28. Westbrook, C. K., Pitz, W. J., Herbinet, O., Curran, H. J. and Silke, E. J., "A Comprehensive Detailed Chemical Kinetic Reaction Mechanism for Combustion of n-alkane Hydrocarbons from n-octane to n-hexadecane", Combustion and Flame, Vol.156-1, pp.181-189, (2009)
29. Magnussen, B. F. and Hjertager, B. H., "On Mathematical Modeling of Turbulent Combustion with Special Emphasis on Soot Formation and Combustion", Proc. Combustion Institute, Vol.16, pp.719-729, (1976)

## CONTACT INFORMATION

Yoshimitsu Kobashi

Department of Mechanical Engineering

Kanazawa Institute of Technology

7-1 Ohgigaoka, Nonoiichi, Ishikawa 921-8501 JAPAN

[yos-wada@neptune.kanazawa-it.ac.jp](mailto:yos-wada@neptune.kanazawa-it.ac.jp)

## ACKNOWLEDGEMENT

This study was supported by Grant-in-Aid for Scientific Research (B) No. 22360091 from the Japan Society for the Promotion of Science.

## ABBREVIATIONS

AHRR	apparent heat release rate	
CA	crank angle	
CN	cetane number	[−]
$dp/d\theta_{max}$	maximum pressure rise rate	[MPa/ deg.CA]
ISF	insoluble fraction (predominantly composed of soot)	
$M_{iC8}$	mass fraction of i-C <sub>8</sub> H <sub>18</sub>	[wt.%]
SOF	soluble organic fraction	
THC	total hydrocarbons	[ppmC]
$X_{O2}$	intake oxygen concentration	[vol.%]
$\eta_c$	combustion efficiency	[%]
$\eta_i$	indicated thermal efficiency	[%]
$\theta_{inj}$	injection pulse timing	[deg.CA ATDC]